

Ag Surface Outflow Kinetics in Ag/AlN Nanomultilayers

Aleksandr V. Druzhinin,* Jolanta Janczak-Rusch, and Claudia Cancellieri*

The heat-induced microstructure evolution of nanomultilayers (NMLs) with metallic components is widely studied due to its critical importance in ensuring the reliable application of these nanomaterials. The thermal degradation of NMLs is controlled by mass transport of one of the NML components from the NML volume to its surface. The outflow occurs at temperatures well below the melting point of metal, offering new opportunities for the engineering of innovative NML-based brazing fillers. A combined experimental-modeling approach for the quantitative analysis of silver (Ag) outflow kinetics in Ag/AlN NMLs is presented. The method is based on in situ monitoring of the X-ray diffraction intensity evolution of Ag acquired from the near-surface region of NML (grazing incidence geometry) upon annealing in the temperature range of 230–425 °C (atmosphere of N₂). The experimental data are compared to model predictions of Ag diffusion. It is assumed that Ag diffusion is driven by the relaxation of residual stresses in Ag nanolayers. Due to the multilayer geometry, the surface outflow kinetics are mainly defined by the kinetics of Ag diffusion along Ag/AlN interphase boundaries. The parameters defining the Ag surface outflow kinetics, i.e., diffusion coefficients and activation energy for diffusion, are derived.

unique physical properties, namely mechanical,^[2] optical,^[3] and magnetic properties^[4] and radiation tolerance.^[5] Superposition of excellent physical properties can be achieved by smart microstructural design (e.g., selection of the bilayer combination,^[6] interfacial design^[7]) coupled with appropriate heat-treatment conditions (temperature, duration, annealing atmosphere^[8,9]).

NMLs are created by periodically stacking nanolayers of selected materials along the substrate's normal direction (bilayer composition). The synthesis of an NML yields a metastable framework owing to the high density of internal interfaces (interphase boundaries, grain boundaries) with associated surface energies. The traditional mechanism for the extra surface energy release is thermal grooving of grain boundaries, originally reported by W.W. Mullins.^[10] In multilayers comprising nanoscale-thick layers, grooving of neighboring grain boundaries on both side

1. Introduction


NMLs, consisting of two or more dissimilar materials, are nanoscale periodic systems that show promising physical properties for various industrial technologies, including microelectronics, catalysis, optics, and energy applications.^[1] The profound interest in these nanomaterials relies on the combination of different

surfaces of the layer is crucial in the degradation of the nanostructure. This process leads to the breakdown of nanolayers and the subsequent coarsening of residual nanolayer fragments, e.g., refs. [11–15]. In accordance with the terminology, grain boundary grooving is a thermally activated process. Therefore, the industrial constraints on the exploitation of NMLs are tightly linked to the kinetics of grooving, which define the upper limits for both the annealing temperature and duration.

However, grain boundary grooving is not the only contributor leading to thermal degradation of NML. Residual stresses in nanolayers typically arise during the NML growth, contributing additional elastic energy to the final nonequilibrium state of the system.^[6,16–20] When depositing polycrystalline nanolayers (which are typical in NMLs), there is classical model describing the compressive–tensile–compressive residual stress transition with an increase in film thickness. This transition is related to the mutual interaction of growing islands and adatom incorporation into the film.^[21] In this evolution, there is a significant contribution of coherency strain and interface stress, which arise from differences in the crystalline structure of the adjoined phases (for more details on interface stress, the reader is referred to ref. [22]). The NML releases the excess elastic energy through plastic deformation, primarily activated at elevated temperatures, known as diffusion creep. In NMLs, the predominant form of creep is diffusion based, involving the mass transport of one of the constituent materials to the NML surface, the so-called surface outflow. Additionally, surface outflow can be driven by capillary forces provided the interface boundary energy is larger

A. V. Druzhinin
Laboratory of Interfaces in Metals
Osipyan Institute of Solid State Physics
Russian Academy of Sciences
Moscow district, 2 Academician Osipyan str., 142432 Chernogolovka,
Russian Federation
E-mail: druzhinin@issp.ac.ru

J. Janczak-Rusch, C. Cancellieri
Laboratory for Joining Technologies and Corrosion
Empa, Swiss Federal Laboratories for Materials Science and Technology
Überlandstrasse 129, 8600 Dübendorf, CH, Switzerland
E-mail: claudia.cancellieri@empa.ch

 The ORCID identification number(s) for the author(s) of this article can be found under <https://doi.org/10.1002/pssa.202300876>.

© 2024 The Authors. physica status solidi (a) applications and materials science published by Wiley-VCH GmbH. This is an open access article under the terms of the Creative Commons Attribution-NonCommercial-NoDerivs License, which permits use and distribution in any medium, provided the original work is properly cited, the use is non-commercial and no modifications or adaptations are made.

DOI: 10.1002/pssa.202300876

than the mean surface energy of the particles formed on the NML surface.^[8]

The surface outflow phenomenon has been thoroughly investigated in NMLs of various material systems (immiscible or semimiscible), e.g., Cu/W,^[9,23] Ag/AlN,^[24] Ag-Cu/AlN,^[25] Ag-Ge/AlN,^[16] Al-Si/AlN,^[26] and Cu/AlN-Al₂O₃.^[27] NMLs. Typically, the outflowing material is a metal phase with a lower melting point (compared to other constituents of an NML) and high diffusion mobility. The kinetics of mass transport to the NML surface are considerable; metal particles of several micrometers in size are formed on the surface of NMLs with less than 10 nm thick nanolayers during relatively short annealing times (<60 min) and at temperatures well below the melting point of the outflowed material. The substantial kinetics of the outflow render these nanomaterials promising as innovative low-temperature brazing fillers for heat-sensitive devices.^[28,29]

However, there is a lack of published works quantitatively determining the outflow kinetics in NML, i.e., the diffusion coefficient of the outflowing metal. This is an important step to properly understand the fundamentals of the thermal stability of an NML system. The complexity of the problem owes to the design of a suitable experimental scheme to analyze the time evolution of the outflowing material volume and to the development of the appropriate diffusion model. Several published works address a similar problem: growth of whiskers on the surface of thin films. In refs. [30,31], the authors analyzed the kinetics of Au and Fe whisker growth by measuring the whisker length and applying an appropriate diffusion model. In the case of Au whiskers, the authors derived the magnitude of the diffusion coefficient. Its activation energy coincided with the activation energy for surface diffusion, proving the capillary driving force for whisker growth. In the case of Fe whiskers, a diffusion approach was developed to reproduce the experimentally observed whisker dimensions. In ref. [32], the diffusion-based problem of stress-driven Sn whisker growth was investigated and experimentally verified. The authors considered the growth of whiskers as the major mechanism of residual stress relaxation in Sn thin films; using the literature data on creep and diffusion, the experimentally derived stress evolution overtime was simulated. These works are the basis for addressing the problem stated in the present work; however, modifications to both the experimental framework and diffusion model are necessary.

Among the NMLs mentioned earlier, the Ag/AlN system is of particular interest for its prominent mechanical and optical properties.^[33] According to the previously published works, these NMLs show a substantial outflow of silver, making them promising brazing fillers for joining technologies.^[8,16,24,34,35] Chiodi et al.^[24] were the first to report a massive Ag outflow upon heating in air at a relatively low temperature (420 °C), which has been recently confirmed by Druzhinin et al.^[8] Oxidation of AlN nanolayers and formation of Al₂O₃ phase result in an increased interface energy. Consequently, the system eliminates Ag/Al₂O₃ interphase boundaries by transporting silver to the NML surface. In an inert atmosphere (e.g., Ar flow) or vacuum, the outflow is reduced due to the absence of the chemical driving force of oxygen; the main driving force is the residual stress relaxation in nanolayers.^[8] A nonreactive atmosphere during annealing is crucial for industrial applications, as it preserves the initially produced phase composition of the NML. Therefore, investigation

of the outflow kinetics upon annealing in a nonreactive atmosphere is of primary importance.

In the present work, the kinetics of Ag surface outflow in Ag/AlN NMLs are experimentally investigated by performing in situ high-temperature grazing incidence X-ray diffraction (GI-XRD) analysis with modeling. The analysis is conducted in nitrogen flow to prevent the oxidation of the AlN nanolayers. For this setup, a diffusion model is developed that considers residual stress relaxation as the principal driving force for the outflow. The time evolution of the outflowing Ag volume is monitored by the diffraction intensity change upon isothermal annealing. The developed diffusion model is applied to experimental data to extract the diffusion coefficient of silver, primarily found to diffuse along the Ag/AlN interphase boundaries. For the first time, the activation energy for diffusion and the temperature dependence of the diffusion coefficient of an outflowing metal filler are experimentally determined.

2. Diffusion Model

Based on previous work,^[8] upon annealing in an inert atmosphere, the driving force of the Ag outflow is not of the capillary nature, and another energy excess has to be considered; the Ag/AlN interface energy is small enough in relation to the Ag surface energy (of Ag crystals on the NML surface), so Ag nanolayers should be stable in the NML volume. The NMLs grown by physical vapor deposition typically possess a nonzero internal stress.^[36] Ag/AlN NMLs are not an exception. Based on previous works,^[16,24] silver nanolayers in Ag/AlN NMLs are specifically under in-plane compressive stress. However, residual stresses are generally not spatially uniform and the experimentally derived stresses are mean values averaged over plenty of grains. In fact, the residual stresses are commonly classified into three types, i.e., macrostress (varying on the millimeter scale; Type I), intergranular microstress (varying on the grain size scale; Type II), and intragranular microstress (imposed by lattice defects; Type III).^[37] Considering the scale of the surface outflow, variation in the macrostresses is of principal importance. Upon film deposition, it is expected that the (macro) regions of compressive and tensile stresses will be formed, resulting in a nonuniform spatial distribution (at a large scale) of in-plane residual stresses. The Ag surface outflow can be considered a diffusion creep. In the regions of compressive and tensile stress, the chemical potential of vacancies decreases and increases, respectively. This gradient of chemical potential causes the flux of vacancies from tensile regions to the compressive ones.^[38] The flux of atoms is the opposite of the flux of vacancies, and diffusion occurs by a vacancy exchange mechanism.

According to refs. [8,34], the channels are formed in the Ag/AlN NML volume upon annealing, which act as pathways for the outflow. In the channels, silver atoms preferentially diffuse along the channel walls by means of surface diffusion. On the NML surface, a discontinuous Ag film initially formed. Afterward, by means of a capillary driving force, bulk-faceted Ag crystals evolved.^[8] Typically, surface diffusion is faster than the diffusion along interface or grain boundaries as well as the bulk diffusion (e.g., surface diffusion coefficient of Au at 400 °C, $4.05 \times 10^{-15} \text{ m}^2 \text{ s}^{-1}$,^[39] is four orders of magnitude

larger than the bulk diffusion coefficient, $5.11 \times 10^{-19} \text{ m}^2 \text{ s}^{-1}$,^[40] surface diffusion coefficient of Ag at 700 °C, $3.61 \times 10^{-10} \text{ m}^2 \text{ s}^{-1}$,^[41] is five orders of magnitude larger than the bulk diffusion coefficient, $7.21 \times 10^{-16} \text{ m}^2 \text{ s}^{-1}$.^[42] This assumption significantly simplifies the diffusion problem, resulting in concise, convenient solutions (e.g., Hwang et al.'s solution of the grain boundary diffusion problem for Harrison's type C diffusion kinetics^[43,44]). In this study, it is supposed that outflow kinetics are limited by diffusion in the Ag nanolayers and not in the channels.

The experimental setup is based on in situ XRD (the grazing incidence scheme; GI-XRD) analysis of the NML annealed in an inert atmosphere (N_2 flow). In this approach, the formation of faceted bulk Ag crystals from a discontinuous silver film is not the limiting factor of the determined outflow kinetics. It is associated with the large area ($\approx 1 \text{ mm}^2$) of experimental analysis by GI-XRD, i.e., the diffracted signal is summed over both the regions containing faceted Ag crystals and the unfaceted Ag film. The kinetics of the outflow are described solely by the diffusion of atoms in the NML bulk, i.e., in the Ag nanolayers and along the channel wall. Thus, the derived diffusion model is based on the relaxation of residual stresses in Ag nanolayers, i.e., it is a principal driving force of the outflow (the capillary driving force of Ag diffusion on the NML surface is neglected). **Figure 1** shows a sketch of the model with the relevant parameters. In the derived model, the gradient of residual stresses along the NML depth is neglected, i.e., mean values of stress are assumed to be the same in each Ag nanolayer.

The change of the Ag volume on the NML surface is

$$\frac{dV}{dt} = J_s(H, t) d_s \Omega \quad (1)$$

where $J_s(H, t)$ is the diffusion flux at the NML surface (H is the NML thickness of $\approx 200 \text{ nm}$);

d_s is the thickness of the diffusing material slab on the side wall of the channel at the NML surface and Ω is the atomic volume of a diffusing substance.

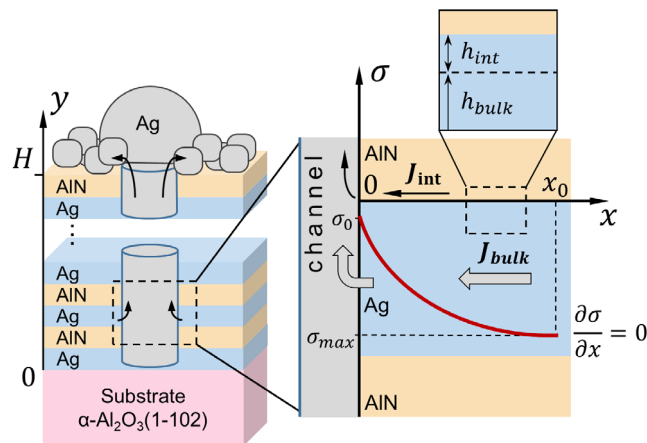


Figure 1. Schematics of diffusion model. J_{int} and J_{bulk} are the diffusion fluxes along interface and in the bulk, respectively. σ is the internal (normal to the channel wall) stress.

The flux in the channel is assumed to be constant along the channel length, i.e., there is no accumulation of material in the channel (the flux divergence is zero; the chemical potential is a linear function of the NML height). If this assumption is not fulfilled, the in-plane stress in the NML would build up, increasing the chemical potential of Ag atoms in the channel, and the driving force for the outflow would disappear.

The $J_s(H) d_s$ term is the atomic flux (number of atoms per unit of time) reaching the NML surface. This amount is the sum of the fluxes supplied by each silver nanolayer:

$$J_s(H, t) d_s = \sum_{i=1}^N J_{s_i} d_{s_i} \quad (2)$$

where N is the amount of Ag nanolayers;

J_{s_i} is the flux supplied by each nanolayer; and

d_{s_i} is the thickness of the diffusing material slab per each Ag nanolayer.

At the junction of each nanolayer with the channel, there is a continuous atomic flux, i.e., the number of incoming atoms is equal to the number of emergent ones. In the 1D problem considered, the atomic flux out of the nanolayer could be expressed as the sum of the bulk (it includes diffusion in the bulk of Ag grains and in Ag/Ag grain boundaries) and interfacial fluxes:

$$J_{s_i} d_{s_i} = -[J_{\text{bulk}_i}(0, t) h_{\text{bulk}_i} + 2J_{\text{int}_i}(0, t) h_{\text{int}_i}] \quad (3)$$

where $J_{\text{bulk}_i}(0, t)$ and $J_{\text{int}_i}(0, t)$ are the bulk and interface atomic fluxes at $x = 0$ in the silver nanolayer, respectively (see Figure 1);

h_{bulk_i} is the “bulk” thickness of the nanolayer; and

h_{int_i} is the model thickness of the interface.

It is assumed that within each nanolayer, the bulk and interfacial fluxes are uniform along the nanolayer thickness, i.e., they do not vary with the y coordinate. The minus sign in Equation (3) is due to the fact that in the Ag nanolayers, atoms diffuse from the region of high compressive stress to the region of low compressive (or zero) stress at the channel–nanolayer border (vacancies diffuse in the opposite direction; see Figure 1). For the chosen direction of the x axis, this flux is negative.

Grain boundaries supply atoms to the channels through a network of interconnected grain boundaries (e.g., “zig-zag” geometry), with the last grain boundary crossing the channel wall. However, in this case, the path is considerably longer than the short-circuit atom supply through the interface and the bulk of the nanolayer. Additionally, only a few grain boundaries cross the wall of the narrow channel (the diameter of a channel is $\approx 20 \text{ nm}$,^[8] assuming that the mean linear size of a grain is similar to the Ag nanolayer thickness, e.g., see refs. [17,45]), so the total area of grain boundary cross sections is expected to be small as well. Additionally, in a real system, compressive stresses could be larger near the grain boundary due to the incorporation of atoms into the grain boundary during deposition.^[21] Large stresses would increase the activation energy of the diffusion of atoms in the grain boundary, substantially lowering the kinetics. Thus, it is expected that even the larger magnitude of the grain boundary diffusion coefficient (compare to the bulk and interface diffusion coefficients; the difference with the interface diffusion coefficient should be considerably smaller) cannot

compensate for the increased diffusion length and the smaller cross-section area, so that the total supply of atoms through the grain boundary network per unit of time is proposed to be negligibly small. In the present work, it is assumed that the diffusing silver atoms are predominantly supplied by bulk diffusion and diffusion through Ag/AlN interfaces ($J_{\text{bulk}_i}(0, t)$ in Equation (3) defines only bulk diffusion in Ag grains).

Thus, the change of the Ag volume on the NML surface is

$$\frac{dV}{dt} = -\Omega_{\text{Ag}} \sum_{i=1}^N [J_{\text{bulk}_i}(0, t)h_{\text{bulk}_i} + 2J_{\text{int}_i}(0, t)h_{\text{int}_i}] \quad (4)$$

where N is the amount of Ag nanolayers,

h is thickness of Ag nanolayer (10 nm), and

Ω_{Ag} is atomic volume of silver.

Since the gradient of residual stresses along the NML depth is neglected, fluxes in each Ag nanolayer are similar.

Diffusion creep is induced by the gradient of the residual stresses between the bulk of the Ag nanolayer and the channel wall. In the present model, the stress normal to the channel wall is assumed to be equal to the critical stress, σ_0 (see Figure 1 and the boundary condition, Equation (16)), while in the bulk of the nanolayer it is compressive (at x_0). The maximum value of stress at x_0 is in the as-deposited state, and this value decreases during the outflow (see Figure 1). In this framework, vacancies diffuse from the channel wall into the bulk of the nanolayer, resulting in an opposite flux of atoms, diffusing by the vacancy exchange mechanism.

The flux of silver atoms in the considered 1D case is

$$J_{\text{Ag}} = -J_v \quad (5)$$

$$J_v = -\frac{c_v D}{kT} \frac{\partial \mu_v}{\partial x} \quad (6)$$

where μ_v is the chemical potential of Ag vacancies;

c_v is the concentration of vacancies; and

D is the vacancy diffusion coefficient.

The chemical potential of vacancies is derived as an additional work to add a vacancy to the region under normal stress (the equation is similar to the chemical potential of an atom, but with an opposite sign^[46]):

$$\mu_v = \mu_0 + \Omega_v \sigma \quad (7)$$

where Ω_v is molar volume of the vacancy, which is similar to the molar volume of the diffusing specie, i.e., $\Omega_v \approx \Omega_{\text{Ag}}$;

σ is the normal stress of the relevant sign (tensile or compressive stress).

Using Equation (5)–(7)

$$J_{\text{Ag}} = \frac{cD\Omega_{\text{Ag}}}{kT} \frac{\partial \sigma}{\partial x} \quad (8)$$

where $c \approx c_v$ is denoted as the concentration of mobile atoms, which is equal to the concentration of diffusing vacancies. The diffusion coefficient of atoms is determined by the diffusion coefficient of vacancies.

The stress gradient within each individual nanolayer (i.e., along the y axis within the nanolayer thickness) is neglected.

Thus, the chemical potential of atoms diffusing in the (denoted) bulk and interface regions are expressed similarly.

Thus, separating the atomic (vacancy) fluxes, Equation (4) is expressed as

$$\begin{aligned} \frac{dV}{dt} &= -\Omega_{\text{Ag}} \left(\sum_{i=1}^N [J_{\text{bulk}_i}(0, t)h_{\text{bulk}_i} + 2J_{\text{int}_i}(0, t)h_{\text{int}_i}] \right) \\ &= -\frac{\Omega_{\text{Ag}}}{kT} (cNh_{\text{bulk}}D_{\text{bulk}}\Omega_{\text{Ag}} + 2cNh_{\text{int}}D_{\text{int}}\Omega_{\text{Ag}}) \left. \frac{\partial \sigma(x, t)}{\partial x} \right|_{x=0} \\ &= -\frac{\Omega_{\text{Ag}}Nh}{kT} \left(\frac{ch_{\text{bulk}}D_{\text{bulk}}\Omega_{\text{Ag}}}{h} + 2\frac{ch_{\text{int}}D_{\text{int}}\Omega_{\text{Ag}}}{h} \right) \left. \frac{\partial \sigma(x, t)}{\partial x} \right|_{x=0} \\ &\equiv -\Omega_{\text{Ag}}NhJ(0, t) \end{aligned} \quad (9)$$

where h is the nanolayer thickness.

The atomic flux at the edge of the channel (at $x = 0$) is

$$\begin{aligned} J(0, t) &= c \left(\frac{h_{\text{bulk}}D_{\text{bulk}}}{h} + 2\frac{h_{\text{int}}D_{\text{int}}}{h} \right) \frac{\Omega_{\text{Ag}}}{kT} \left. \frac{\partial \sigma(x, t)}{\partial x} \right|_{x=0} \\ &\equiv cD_{\text{eff}} \frac{\Omega_{\text{Ag}}}{kT} \left. \frac{\partial \sigma(x, t)}{\partial x} \right|_{x=0} \end{aligned} \quad (10)$$

where D_{eff} is an effective diffusion coefficient, which takes into account bulk diffusion and diffusion along interfaces.

Essentially, c equals bulk concentration c_{bulk} of the solid ($c = c_{\text{bulk}}$), which is considered as an inverse atomic volume, Ω^{-1} . Interface concentration, c_{int} , can be defined:

$$c_{\text{int}} = c_{\text{bulk}}h_{\text{int}} \quad (11)$$

Generally, the diffusion coefficient depends on the stress magnitude by adding the term $\frac{|\sigma_{\text{el}}|\Omega_{\text{at}}}{3N_A}$ (energy units) to the activation energy, where N_A is the Avogadro constant and Ω_{at} is the molar volume.^[47] According to the literature data refs. [16,24], the average compressive stress magnitude in Ag nanolayers in Ag/AlN NMLs is <400 MPa (absolute value). Indeed, by means of XRD, the derived magnitude of the average in-plane residual stress in the as-deposited Ag nanolayers is -340 ± 50 MPa (compressive; for details of the calculation, see Supporting Information, Part I), in agreement with previously reported values. Thus, the maximum value of the correction to the average activation energy is less than 0.03 eV (based on the identity shown earlier). Typically, tensile stress decreases the activation energy, whereas compressive stress increases it. Definitely, due to the spatial distribution of the stresses, the activation energy undergoes larger changes due to the correction term, fluctuating around the mean value. However, it is assumed that these changes are short-range and, for the present problem, do not substantially alter the atomic flux.

Plasticity releases the elastic part of the strain. For the film (NML) constrained by the substrate, the total strain is fixed. Thus, the total strain rate in each Ag nanolayer is

$$\dot{\epsilon} = \dot{\epsilon}_{\text{el}} + \dot{\epsilon}_{\text{pl}} = 0 \quad (12)$$

$\dot{\epsilon}$ is the total strain rate;

$\dot{\epsilon}_{\text{el}}$ is the elastic strain rate; and

$\dot{\epsilon}_{\text{pl}}$ is the plastic strain rate.

The plastic strain rate is determined by the divergence of the atomic flux:

$$\dot{\epsilon}_{pl} = -\Omega_{Ag} \cdot \nabla J \quad (13)$$

In the studied 1D problem, taking into account Equation (13), the final equation for the stress evolution is obtained:

$$\frac{\partial \sigma}{\partial t} = R \frac{\partial^2 \sigma}{\partial x^2} \quad (14)$$

$$R = \frac{E c_{bulk} D_{eff} \Omega_{Ag}^2}{(1 - \nu) k T} \quad (15)$$

where E and ν are the Young modulus (85 GPa) and Poisson ratio (0.37) of silver, respectively.

In the derived equation, the term R is artificially introduced to facilitate further notations, when solving the differential equation. However, it can formally be considered as a kinetics coefficient, indicating the kinetics of the internal stress change.

The boundary conditions are similar to those proposed by Pei et al. in ref. [32] for modeling the growth of Sn whiskers. At the channel boundary, i.e., at $x=0$, the stress is equal to a critical value. This critical stress is lower than the magnitude of the average stress in the nanolayer and induces the gradient of stress, which initiates the flow of Ag atoms (vacancies). On the contrary, the zero flux condition is imposed away from the channel. This is based on the spatial variation of macrostress, which can undergo a change from compressive to tensile. Thus, the volume region responsible for the supply of a silver particle driven by the compressive stress relaxation is bound. Additionally, this condition reflects that the fluxes of neighboring groups of channels do not overlap with each other. Precisely, each group of channels is supplied by a specific volume of NML, with a specific in-plane area. These volumes are assumed not to overlap, i.e., neighboring channels do not influence each other. Thus, there is a flux of Ag atoms toward the channel until the homogeneous distribution of the stress (it equals the critical value) is achieved.

Boundary conditions are defined as

$$\sigma(0, t) = \sigma_0 \text{ (critical stress)} \quad (16)$$

$$\left. \frac{\partial \sigma(x, t)}{\partial x} \right|_{x=x_0} = 0 \text{ (zero flux condition)} \quad (17)$$

where x_0 is the distance away from the channel (see Figure 1).

Initial conditions include the uniformity of stress throughout the nanolayer volume (spatial distribution):

$$\sigma(x, 0) = \sigma_{max} \quad (18)$$

The solution for the derived nonlinear partial differential equation is similar to the solution of the diffusion equation for the plane sheet problem.^[48] The solution obtained by the method of the Laplace transformation is

$$\sigma(x, t) = (\sigma_0 - \sigma_{max}) \left[\sum_{n=0}^{\infty} (-1)^n \operatorname{erfc} \left(\frac{2x_0(n+1) - x}{2\sqrt{Rt}} \right) + \sum_{n=0}^{\infty} (-1)^n \operatorname{erfc} \left(\frac{2x_0n + x}{2\sqrt{Rt}} \right) \right] + \sigma_{max} \quad (19)$$

The series converges quite rapidly, and the 10^{-6} difference in stress values is already achieved at $n = 35$.

According to Equation (10), the atomic flux is

$$J(0, t) = \frac{(\sigma_0 - \sigma_{max}) \sqrt{R}(1 - \nu)}{\sqrt{\pi t E \Omega_{Ag}}} \left[\sum_{n=0}^{\infty} (-1)^n \exp \left(-\frac{x_0^2(n+1)^2}{Rt} \right) - \sum_{n=0}^{\infty} (-1)^n \exp \left(-\frac{x_0^2 n^2}{Rt} \right) \right] \quad (20)$$

Integrating Equation (9) with the initial condition $V(0) = 0$ and the selected amount of terms, N , the time evolution of Ag volume is determined:

$$V(t) = -Nh \frac{(\sigma_0 - \sigma_{max}) \sqrt{R}(1 - \nu)}{E} \left(\sum_{n=0}^N (-1)^n \left[\frac{2}{\sqrt{\pi}} \sqrt{t} \exp \left(-\frac{x_0^2(n+1)^2}{Rt} \right) + \frac{2x_0(n+1)}{\sqrt{R}} \operatorname{erf} \left(\frac{x_0(n+1)}{\sqrt{Rt}} \right) \right] - \sum_{n=0}^N (-1)^n \left[\frac{2}{\sqrt{\pi}} \sqrt{t} \exp \left(-\frac{x_0^2 n^2}{Rt} \right) + \frac{2x_0 n}{\sqrt{R}} \operatorname{erf} \left(\frac{x_0 n}{\sqrt{Rt}} \right) \right] - \sum_{n=0}^N (-1)^n \frac{2x_0}{\sqrt{R}} \right) \quad (21)$$

The principal assumptions made are summarized as follows: 1) the kinetics of the surface outflow are defined by diffusion creep in Ag nanolayers, and atoms diffuse by the vacancy exchange mechanism; 2) the residual stress relaxation in Ag nanolayers is the principal driving force of the outflow, and the outflow kinetics are limited by diffusion in the nanolayers; 3) the gradient of residual stresses along the NML depth is neglected, as well as the gradient within each individual nanolayer; 4) bulk and interfacial fluxes are uniform along the nanolayer thickness, i.e., they do not change with the y coordinate; 5) the diffusing silver atoms are dominantly supplied by bulk self-diffusion and diffusion along Ag/AlN interfaces. 6) The spatial changes in activation energy due to the distribution of macrostresses are short range and do not change the atomic flux.

Figure 2 shows the model $V(t)$ as a function of σ_{max} and R parameters ($x_0 = 1 \mu\text{m}$, $\sigma_0 = 0$, $n = 30$, $N = 20$, $h = 10 \text{ nm}$). It follows that the increase of the compressive stresses in nanolayers σ_{max} results in a larger outflow, i.e., a larger saturation value, which is in agreement with the nature of the diffusion creep (Figure 2a). Apparently, the outflow kinetics are sensitive to the change of R , since the diffusion coefficient D_{eff} is the basis of this parameter (Figure 2b).

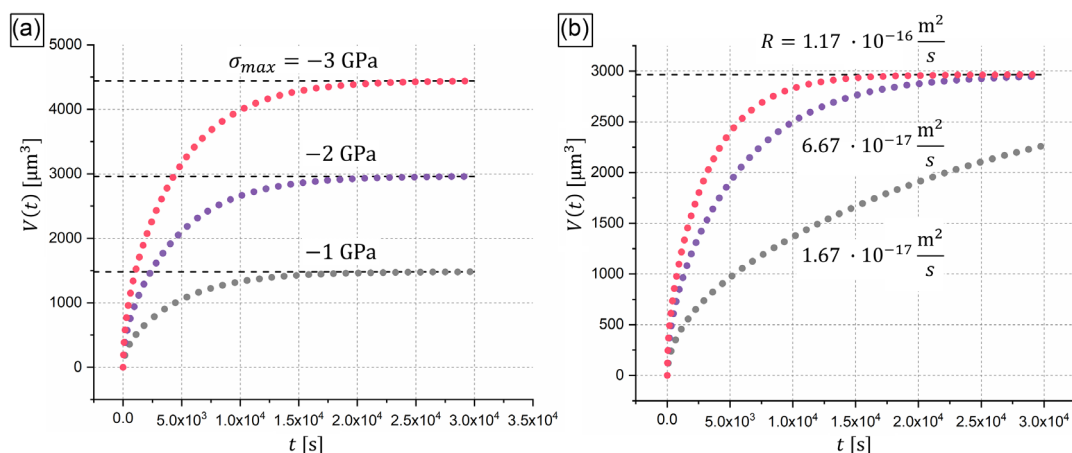


Figure 2. Model time dependence of the outflowing material volume for different values of σ_{\max} and R . The surface outflow kinetics is calculated for a) three magnitudes of σ_{\max} with $R = 8.34 \times 10^{-15} \text{ m}^2 \text{ s}^{-1}$ held constant and b) for three magnitudes of R with $\sigma_{\max} = -2 \text{ GPa}$ held constant.

3. Results and Discussion

The cross section and top surface microstructure of as-deposited Ag/AlN NMLs were previously shown in Figure 1 in ref. [8]. The as-deposited NMLs exhibit in-plane and out-of-plane textures with the crystallographic orientation relationship $\text{Ag}\{111\} \langle 10\text{-}1 \rangle \parallel \text{AlN}\{0001\} \langle 2\text{-}1\text{-}10 \rangle$, similar to previous works.^[8,24] In Figure 3a, θ - 2θ XRD scans of the as-deposited state and during in situ heating till 750°C are shown (Bragg–Brentano geometry). The scan of the as-deposited NML expectedly shows only reflections belonging to the Ag {111} and AlN {0001} families of planes, according to the crystallographic texture. At 750°C , the intensities of the Ag(111) and Ag(222) peaks decrease. At the same time, the sharp Ag(200) peak arises from the Ag phase, which is not consistent with the as-deposited crystallographic texture. The observed evolution of the peaks indicates the outflow of silver to the NML surface upon annealing, when the polycrystalline Ag particles are formed on the NML surface. In Figure 3b, the evolution of $d_{(111)}$, the interplanar Ag(111) spacing change

upon heating and cooling of the sample is shown. The $d_{(111)}$ evolution of the NML upon cooling down (black points) follows the linear thermal expansion law with a coefficient of thermal expansion ($2.53 \times 10^{-5} \text{ }^\circ\text{C}^{-1}$) similar to the one of bulk silver ($2.06 \times 10^{-5} \text{ }^\circ\text{C}^{-1}$, ref. [49]). The anomalous increase in the interplanar distance change is observed at a temperature of $\approx 380^\circ\text{C}$ (highlighted by an ellipse), indicating the onset of the Ag surface outflow. This discrepancy with the linear thermal expansion could arise due to the formation of small islands of the outflowing material on the NML surface, which are strained by the AlN top nanolayer due to the lattice parameter mismatch and the surface and interface stresses.^[22] At a temperature of $\approx 700^\circ\text{C}$ interplanar spacing follows again the linear trend, indicating that the outflow process is completed. These observations confirm that the outflow process is energy activated, and it has to be described by diffusion laws. Additionally, the ongoing outflow is observed by monitoring the shape of the diffraction peaks, which become narrower with the annealing duration. The time evolution of the full width at half maximum of the Ag(111) peak is shown in

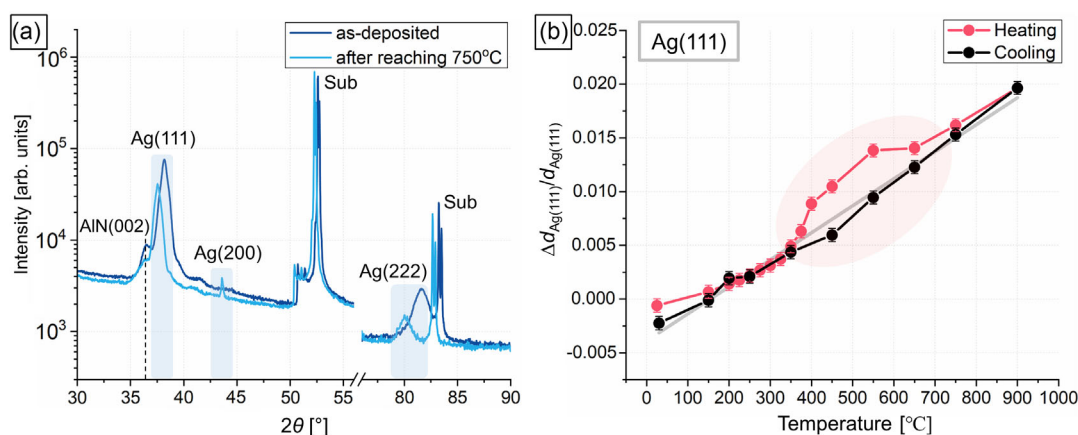


Figure 3. a) XRD spectrum in the Bragg–Brentano geometry of the as-deposited NML and b) the evolution of interplanar Ag(111) spacing change (in relation to the bulk $d_{\text{Ag}(111)} = 2.359 \text{ \AA}$) upon heating from room temperature to 900°C as determined in situ by XRD analysis. The gray linear function is a fit of data points derived upon cooling of the sample (black points). The estimated coefficient of thermal expansion is $2.53 \times 10^{-5} \text{ }^\circ\text{C}^{-1}$ is similar to the one for bulk silver, $2.06 \times 10^{-5} \text{ }^\circ\text{C}^{-1}$.^[49]

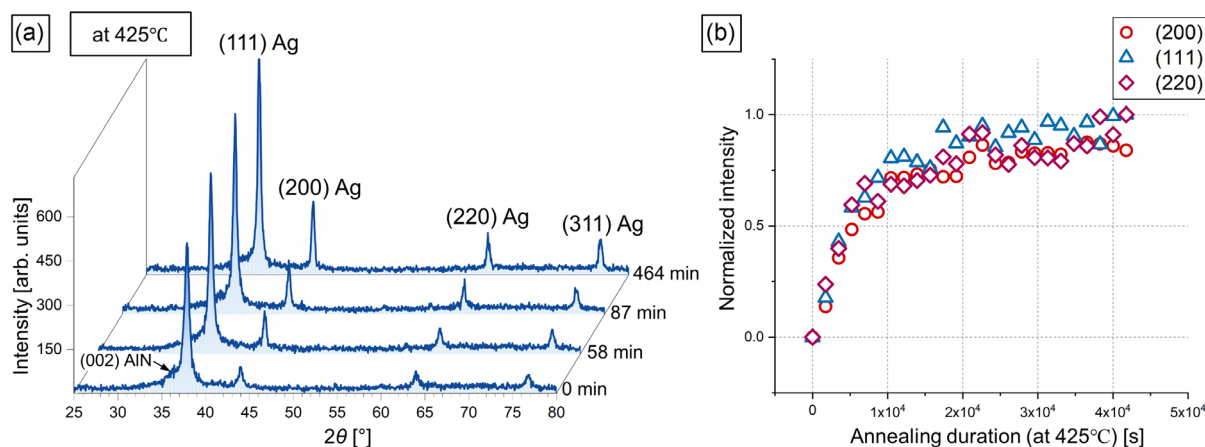


Figure 4. a) GI XRD spectra of the as-deposited sample and the sample upon annealing at 425 °C. b) Normalized intensity evolution of (111), (200), and (220) Ag peaks.

Figure S2, Supporting Information, Part II. This fact highlights the grain coarsening of the analyzed silver phase, which is related to the gradual growth of silver particles on the NML surface.

In Figure 4a, GI-XRD spectra (the incidence angle is 5°) of the as-deposited sample and the sample annealed at 425 °C are shown. The use of more surface sensitive GI diffraction instead of the standard Bragg–Brentano geometry helps to capture the onset of Ag outflow. Moreover, in this configuration, there are no peaks coming from the substrate, which may complicate the data interpretation. The as-deposited GI scan shows several silver reflections, i.e., the minority of grains that are misoriented with respect to the dominant crystallographic relationship (texture) contribute to the diffracted intensity. Heat treatment activates the Ag surface outflow. The silver particles formed on the NML surface are essentially polycrystalline, as confirmed by the emergence of additional peaks, e.g., Ag(200) (it was also disclosed by XRD in the previous work, ref. [24]). The increase in the intensity of Ag reflections is proportional to the amount of silver transported to the NML surface upon outflow. The intensity evolution of (200), (111), and (220) silver reflections was monitored (peak intensity in the as-deposited state is subtracted). According to the peak normalized intensity evolution in Figure 4b, the trend of the intensity rise does not appreciably depend on the chosen Ag reflection, confirming the polycrystallinity of the outflowed silver. Due to the smaller contribution of the background signals and the higher intensity of the peak, the Ag(111) reflection evolution was chosen to derive the kinetics of the Ag volume evolution induced by the outflow.

The survey scanning electron microscopy (SEM) images of NMLs after annealing in the GI XRD machine are shown on Figure 5a–c. The surface outflow results in the formation of narrow stripes covered by Ag atoms (highlighted in the inset of Figure 5a). Initially, silver atoms diffuse to the top surface in the region of the stripes. Afterward, driven by the minimization of surface energy (capillary driving force), silver atoms aggregate into bulk particles (insets in Figure 5a–c). The stripes are more pronounced in the sample after annealing at 230 °C. On the contrary, in the sample annealed at 425 °C, the bulk Ag particles are mainly formed. This is not surprising since the outflow

kinetics are determined by the silver diffusion, and saturation is reached at lower annealing duration. As it was mentioned in the model description (Section 2), diffusion of Ag atoms takes place through the channels formed in the NML volume. The cross-section study also revealed the formation of channels in the investigated Ag/AlN NMLs (highlighted by arrows in Figure 5d). These channels are the pathways for diffusing silver atoms.

The derived diffusion model includes the characteristic length x_0 , which bounds the outflow area of a single channel. This length is related to the as-deposited distribution of residual macrostresses and is assumed to be independent of the annealing temperature and duration. The Ag mass conservation upon outflow is used to assess the magnitude of x_0 . The size of Ag particles on the NML surface is defined by the volume of the underlying nanolayers. It is assumed that, on average, each particle is formed out of the Ag atoms contained in a stripe of thickness d (schematically highlighted in the inset of Figure 3c), which is determined by the sum of the mean diameter of a particle and the mean distance between the neighboring particles (the doubled half-distance between the particles). For the calculation, images of the 425 °C annealed sample were used, since at this temperature the most of the outflowing silver is aggregated into Ag crystals (and the XRD intensity is saturated). Inside the NML volume, silver atoms are assumed to diffuse into the channel from opposite sides of the stripe, i.e., the rectangular region with the doubled x_0 range is considered. Comparing the mean volume of the outflowing silver particles (mean radius is $\approx 0.5 \mu\text{m}$) with the rectangular region of the $(2x_0 \times d)$ area and the (20×10) nm height (20 is the number of nanolayers in the NML stack), the x_0 estimate is $1.10 \mu\text{m}$ (d is $\approx 1.19 \mu\text{m}$).

The GI XRD intensity is proportional to $2V(t)$, since the factor of 2 arises from the assumption that diffusion takes place from both sides of the stripe (within the derived 1D model). The stress difference multiplied by the proportionality coefficient A , $2A(\sigma_0 - \sigma_{\text{max}})$. The term A takes into account the proportionality of the X-ray intensity to the total outflowing volume in the analyzed region. A and R are the fitting parameters. The number of terms in a series (Equation (21)) is 35. In Figure 6a–c, fits to the

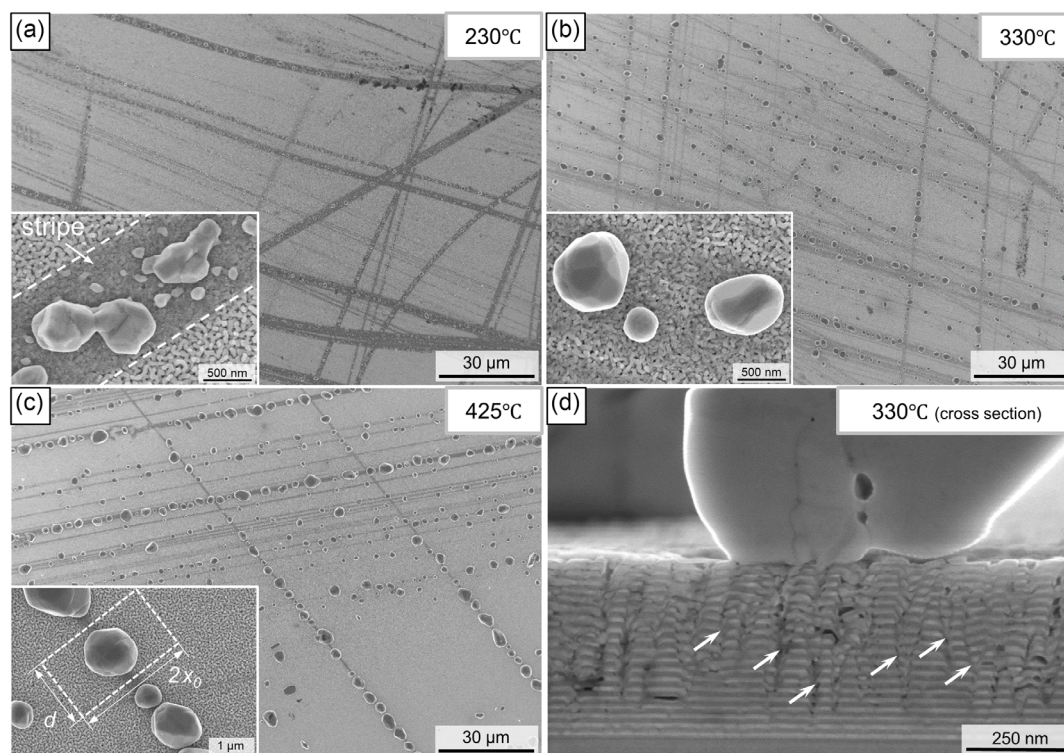


Figure 5. Surface images of NMLs annealed at a) 230 °C (for 1392 min), b) 330 °C (for 1392 min), and c) 425 °C (for 696 min) in the N₂ flow, and d) the cross-section image of the NML annealed at 330 °C with highlighted channels.

experimental data related to three annealing temperatures (230, 330, 425 °C) are presented.

The values of the diffusion coefficient (and the activation energy) can be calculated from the magnitudes of R derived by fitting the data. The melting point of bulk Ag is ≈ 961 °C (based on the high temperature-XRD results, silver in nanolayers does not melt up to 900 °C), i.e., the largest homologous annealing temperature is 0.44 (≈ 425 °C/961 °C). Under these conditions, bulk diffusion is essentially frozen. Considering the small thickness of the nanolayers, i.e., the magnitude of $2\frac{h_{\text{int}}}{h}$ in Equation (10) is relatively large, the contribution of the interface diffusion to the amount of atoms transported to the channel per unit of time is expected to be dominant. Thus, the first term in D_{eff} is neglected. It is assumed that the magnitudes of c_{bulk} (c equals c_{bulk} ; see Section 2) and $2\frac{h_{\text{int}}}{h}$ are essentially independent of the annealing temperature and are inherent to the initial state of Ag nanolayers. The activation energy can be derived from the Arrhenius plot in coordinates of $\ln\left(c_{\text{bulk}} \frac{2h_{\text{int}}D_{\text{int}}}{h}\right) = f(1/T)$ (Figure 6d).

The derived value of activation energy is 0.57 ± 0.01 eV. Based on the published data, the bulk Ag self-diffusion activation energy is 2.14 eV in ref. [42] and 1.91 eV in ref. [50]. The derived magnitude of activation energy $E_{\text{A}}^{\text{int}}$ is considerably smaller than that of bulk diffusion, confirming the prevalence of interface diffusion over bulk diffusion (according to the discussion of the model in Section 2, grain boundary diffusion is not considered). Generally, the first and second terms in D_{eff} are expected to be of

similar magnitude only for thin nanolayers in the narrow range of high temperatures close to the melting point of the diffusing substance. The magnitude of $E_{\text{A}}^{\text{int}}$ is also smaller than the magnitude of the grain boundary diffusion activation energy (the values reported in the literature are 0.87 eV in ref. [42]; 0.704, 0.772, and 0.837 eV in ref. [51]). It presumes that the role (weight in the total flux) of the grain boundary diffusion is not dominant and the diffusion through the interfaces prevails, supporting the assumptions in Section 2. In ref. [52], Gumbsch et al. investigated the properties of the Ag/Ni interface and found out that the activation energy for the Ag vacancy formation is considerably smaller (by up to 1 eV) than in the Ag bulk. The vacancy formation energy in the Ag bulk is 1.06,^[53] 1.16,^[54] and 0.93 eV,^[52] i.e., at the Ag/Ni interface, this energy could be as low as ≈ 0.20 eV at the structurally relaxed interface regions. The activation energy for diffusion by the vacancy mechanism is the sum of the formation energy and the migration energy. The vacancy migration energy on the Ag (111) atomic plane is, e.g., 0.404 eV.^[55] Applying a similar discussion to the case of the Ag(111)/AlN(0001) interface, the estimated value of activation energy can be around 0.60 eV, which is close to the experimentally derived magnitude of 0.57 ± 0.01 eV. In the literature, there is a lack of data on the interstitial formation energy of silver. Referring to the similar face-centered cubic cell of Cu, the interstitial formation energy is up to 1.5 times larger than the energy to form a vacancy.^[56–58] According to Bian et al.^[59] migration energy of interstitials along Ag/AlN interfaces is expected to be large as well due to the considerable magnitude of the work

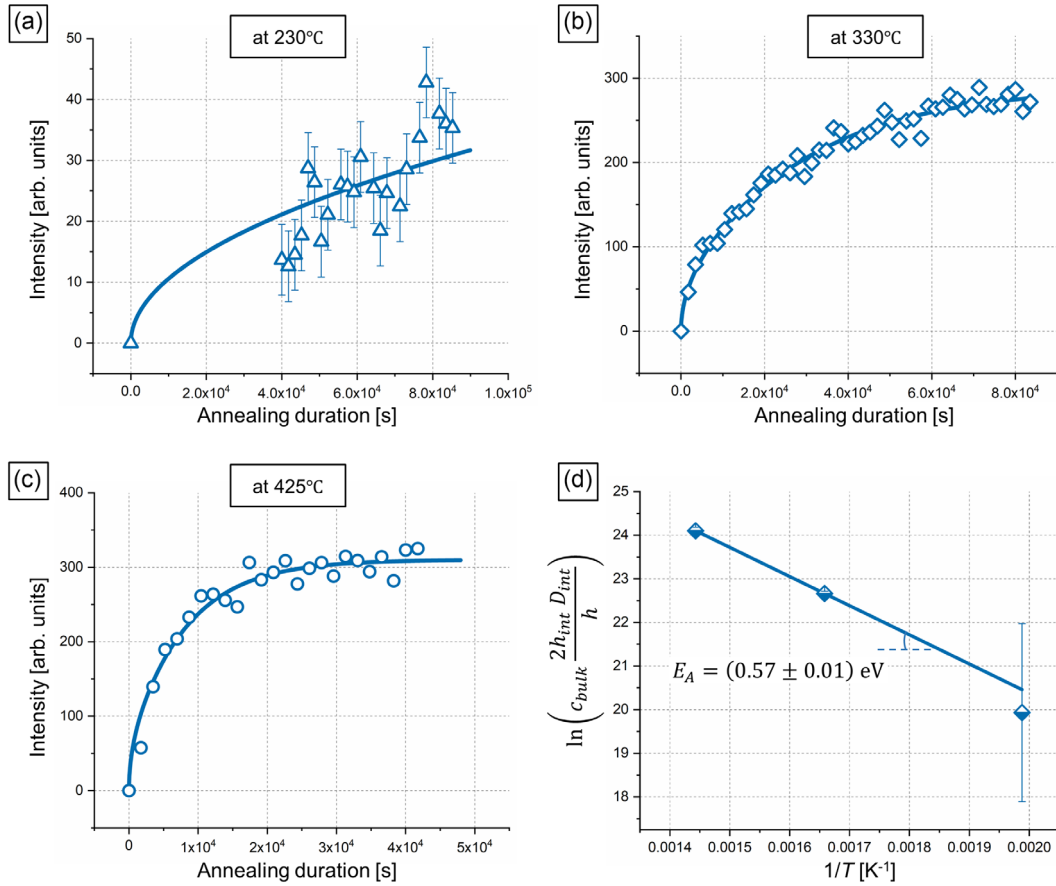


Figure 6. a–c) Evolution of the Ag (111) peak intensity with the annealing duration and d) the Arrhenius plot used to derive the activation energy. The symbol sizes at 330 and 425 °C are larger than the error bars.

of adhesion ($\approx 3.00\text{--}3.50 \text{ J m}^{-2}$). Thus, the vacancy mechanism of diffusion in the near-interface region is proposed.

Proceeding further with the experimental diffusion data analysis, the determination of the temperature dependence of the diffusion coefficient could be obtained. However, in the present case, a proper determination of the D_{int}^0 term is complicated. The complexity arises from the lack of knowledge of the interfacial concentration of mobile silver atoms, c_{int} . In Equation (10) and (11), atomic concentration at the interface is expressed by c ($= c_{\text{bulk}}$) and h_{int} . However, it could be smaller than the planar atomic density of the ideal (111) Ag atomic plane ($\approx 1.44 \times 10^{19} \text{ m}^{-2}$). In ref. [60], Amram et al. investigated the kinetics of the Ni grain boundary groove evolution and determined the $c_s D_s$ term, which was $10^4\text{--}10^6$ times smaller than the published surface diffusivity of Ni. Similarly, discrepancies of several orders of magnitude were found in ref. [30] in the pre-exponential factors D_0 of the Au diffusion coefficient (the experimentally derived one and the one published in the literature for the Au surface diffusion). Thus, in the present model, the coefficient k (< 1) should be introduced in the right-hand side of Equation (8) and (11), i.e., $J_{\text{int}} = \frac{k c D \Omega_{\text{Ag}}}{kT} \frac{\partial \sigma}{\partial x}$ and $c_{\text{int}} = k c_{\text{bulk}} h_{\text{int}}$, respectively. In Figure 6d, the values at the vertical axis have to be modified as $c_{\text{bulk}} k \frac{2h_{\text{int}} D_{\text{int}}}{h}$. The magnitude of h_{int} is fixed and equaled to the width of the Ag(111)/AlN(0001) interface of

$\approx 2 \text{ \AA}$ with the maximum work of adhesion derived by Bian et al. in ref. [59]. Concentration c_{bulk} is of 10^{28} m^{-3} order ($\approx 5.73 \times 10^{28} \text{ m}^{-3}$ for Ag; $c_{\text{bulk}} = \Omega_{\text{Ag}}^{-1}$, where $\Omega_{\text{Ag}} = 1.71 \times 10^{-29} \text{ m}^3$). Taking coefficient $k \approx 10^{-4}$ ($h = 10 \text{ nm}$), diffusion coefficients of Ag diffusion along Ag(111)/AlN(0001) interfaces are estimated as: $1.98 \times 10^{-15} \text{ m}^2 \text{ s}^{-1}$ at 230 °C, $3.04 \times 10^{-14} \text{ m}^2 \text{ s}^{-1}$ at 330 °C, $1.28 \times 10^{-13} \text{ m}^2 \text{ s}^{-1}$ at 425 °C. By an Arrhenius plot analysis, the pre-exponential factor is $D_{\text{int}}^0 = (2.01 \pm 0.36) \times 10^{-9} \text{ m}^2 \text{ s}^{-1}$ is determined. For comparison, Ag grain boundary self-diffusion at 425 °C is $1.55 \times 10^{-12} \text{ m}^2 \text{ s}^{-1}$, i.e., around one order of magnitude larger.^[42]

The choice of the k magnitude can be physically rationalized in the following way. Considering the vacancy diffusion mechanism, the concentration of mobile atoms at the interface equals the concentration of interfacial vacancies, i.e., $c_{\text{int}} \approx c_{\text{int}}^{\text{v}}$, $c_{\text{bulk}} \approx c_{\text{bulk}}^{\text{v}}$. Assuming the residual stresses at the Ag/AlN interface to be relatively small, the vacancy formation energy changes slightly. Equation (11) can be expressed in the following way:

$$c_{\text{int}}^{\text{v}} = k c_{\text{bulk}}^{\text{v}} h_{\text{int}} \quad (22)$$

$$\frac{c_{\text{int}}^{\text{at}}}{\exp\left(-\frac{E_{\text{int}}^{\text{at}}}{kT}\right)} = k \frac{c_{\text{bulk}}^{\text{at}}}{\exp\left(-\frac{E_{\text{bulk}}^{\text{at}}}{kT}\right)} h_{\text{int}} \quad (23)$$

$$k^{-1} = \frac{c_{\text{bulk}}^{\text{at}} h_{\text{int}}}{c_{\text{int}}^{\text{at}}} \frac{\exp\left(-\frac{E_{\text{V}}^{\text{int}}}{kT}\right)}{\exp\left(-\frac{E_{\text{V}}^{\text{bulk}}}{kT}\right)} \quad (24)$$

$$k \approx \exp\left(-\frac{E_{\text{V}}^{\text{bulk}} - E_{\text{V}}^{\text{int}}}{kT}\right) \quad (25)$$

where $E_{\text{V}}^{\text{int}}$ and $E_{\text{V}}^{\text{bulk}}$ are the Ag vacancy formation energy at the Ag/AlN interface and in the Ag bulk, respectively;

$c_{\text{int}}^{\text{at}}$ and $c_{\text{bulk}}^{\text{at}}$ are atomic concentrations at the interface and in the bulk, respectively, derived through the molar volume of material. The following equality $c_{\text{int}}^{\text{at}} = c_{\text{bulk}}^{\text{at}} h_{\text{int}}$ is used.

When $E_{\text{V}}^{\text{bulk}} \approx E_{\text{V}}^{\text{int}}$, k is approximately equal to the unit, $k \approx 1$. Thus, the introduction of this coefficient can be rationalized on the basis of the change of the vacancy formation energy at the interface in relation to the bulk of the Ag nanolayer. Citing again the work of Gumbsch et al.^[52] the vacancy formation energy at the interface (Ag/Ni in the case of authors) can vary substantially due to the distortions and relaxations of the interface atomic structure; there are regions at the interface with vacancy formation energies < 0.5 eV. The value of 0.5 eV is used to estimate $E_{\text{V}}^{\text{int}}$; the bulk value of the formation energy $E_{\text{V}}^{\text{bulk}}$ is ≈ 1 eV. For the temperature range of 230–425 °C, the range of the k value is 10^{-4} – 10^{-5} , which agrees well with the discrepancies among the values of cD term and the diffusion coefficients D found in the literature (e.g., mentioned earlier in refs. [30,60]).

Certainly, in this approach, the k magnitude depends on the temperature, which has to be considered in the derivation of the activation energy for diffusion. However, in the present study, the temperature dependence of k in the determination of activation energy of diffusion was not considered since the correct magnitude of $E_{\text{V}}^{\text{int}}$ for the investigated Ag(111)/AlN(0001) interface is essentially unknown (even for the case of Ag/Ni in ref. [52], this value is smeared). Thus, it may introduce an additional error, which, together with other unavoidable assumptions made in the model, would not gain any significant accuracy in the present determination of the diffusion coefficient. Nevertheless, the proper postulation of the interface parameters such as concentration or thickness is important as they are related to the diffusion models used in the interface diffusion experiments (e.g., ref. [61]).

4. Conclusion

In this study, the kinetics of Ag outflow in Ag/AlN NMLs upon annealing were investigated. In situ analysis by high temperature-XRD showed that the Ag surface outflow is an energy-activated process, and its kinetics can be described by diffusion laws. To experimentally determine the outflow kinetics, in situ GI-XRD analysis of the NML was conducted upon annealing up to 425 °C in an inert atmosphere (nitrogen flow). Based on the experimental setup, a relevant diffusion model was developed that considers residual stress relaxation as the main driving force for the outflow (applicable for annealing in a nonreactive atmosphere). This model is based on the lateral distribution of residual stresses in Ag nanolayers near the hollow channels, which are formed in Ag/AlN NMLs at the onset of annealing. It assumes that the gradient of residual compressive stresses drives the flow

of atoms toward these channels. Afterward, the atoms diffuse to the NML surface through surface diffusion along the channel walls, preventing the accumulation of silver in the channels and building up in-plane stresses. Due to the higher kinetics of surface diffusion, the outflow kinetics are limited by the diffusion of silver atoms in the Ag nanolayer. For the range of annealing temperatures used (230–425 °C), the bulk Ag diffusion is essentially frozen. The supply of atoms diffusing through the Ag grain boundaries is assumed to be negligible, owing to the large diffusion path through a network of connected grain boundaries in nanograined Ag layers. Thus, the derived diffusion coefficient is mainly defined by the diffusion along the short-circuit Ag(111)/AlN(0001) interfaces (based on the strong crystallographic texture in the as-deposited NMLs). The thus-derived interface diffusion coefficient is $D_{\text{Ag}(111)/\text{AlN}(0001)}^{\text{int}} = (2.01 \pm 0.36) \times 10^{-9} \exp\left(-\frac{(0.57 \pm 0.01)\text{eV}}{kT}\right) \frac{\text{m}^2}{\text{s}}$.

5. Experimental Section

Ag/AlN NMLs were deposited at room temperature on single-crystalline $\alpha\text{-Al}_2\text{O}_3$ (1-102) substrates (*R*-cut) by magnetron sputtering in a high vacuum chamber (base pressure $< 10^{-6}$ Pa) from two confocally arranged, unbalanced magnetrons equipped with targets of pure Ag (99.99%) and Al (99.99%). Before insertion into the sputter chamber, the sapphire substrates were ultrasonically cleaned using acetone and isopropanol. Prior to the deposition, possible surface contamination on the substrate surface was removed by Ar^+ sputtering for 5 min by applying radio-frequency bias of -100 V. The Ar pressure was 0.5 Pa (the flow rate of Ar was $15 \text{ cm}^3 \text{ min}^{-1}$) during Ag and AlN deposition. During AlN deposition, a flux of nitrogen was introduced (the flow rate of N_2 was $7 \text{ cm}^3 \text{ min}^{-1}$). First, a 10 nm thick AlN layer was deposited on the sputter-cleaned substrate surface. Next, NML consisting of twenty 10 nm Ag/10 nm AlN bilayers was deposited on top.

In situ XRD analyses of the samples upon annealing were conducted on the PANalytical X'Pert-Pro diffractometer system equipped with the Cu $K\alpha_{1,2}$ radiation at 40 kV/40 mA and Anton Paar XRK 900 sample holder. In the present work, two types of diffraction methods were used. The first type was based on the traditional recording of θ - 2θ scans in the Bragg-Brentano geometry (high temperature-XRD) with the sample continuously heated up from room temperature to 900 °C and afterward cooled down back to room temperature. The second type was the GI-XRD with the incidence angle of 5°. In this method, three samples were isothermally annealed at different temperatures of 230 °C (for 1392 min), 330 °C (for 1392 min), and 425 °C (for 696 min). The smaller annealing duration of 696 min was selected due to the early saturation of the Ag volume at the NML surface. In both methods, each θ - 2θ scan was acquired for 30 min in the 2θ range from 10° to 90°. The time interval between neighboring scans in the high temperature-XRD analysis was 12 min. In the GI-XRD analysis, each new spectrum was recorded right after the previous one was finished. Upon analysis in each diffraction geometry, samples were annealed in the N_2 flow ($100 \text{ cm}^3 \text{ min}^{-1}$) in the specimen holder, initially evacuated by a membrane pump. Nitrogen was used to minimize the background scattering effect due to the smaller X-ray scattering in comparison with Ar. Surface and cross-section imaging was done by SEM. For cross-section analysis, the samples were prepared by a Hitachi IM4000Ar ion-milling system (acceleration voltage of 6 kV, discharge voltage of 1.5 kV, swing angle of $\pm 30^\circ$).

Supporting Information

Supporting Information is available from the Wiley Online Library or from the author.

Acknowledgements

The reported study is funded by Russian Science Foundation (RSF), project no. 22-72-00006 (<https://rscf.ru/en/project/22-72-00006/>). The authors acknowledge Dr. Lars P.H. Jeurgens for fruitful discussions, Dr. Mirco Chiodi for the deposition of the nanomultilayers, Dr. Frank Moszner for the SEM characterization, and N. N. for help with data fitting.

Conflict of Interest

The authors declare no conflict of interest.

Data Availability Statement

The data that support the findings of this study are available from the corresponding author upon reasonable request.

Keywords

interface diffusions, metal outflows, multilayers, residual stresses, X-ray diffractions

Received: November 22, 2023

Revised: January 16, 2024

Published online:

- [1] A. Sáenz-Trevizo, A. M. Hodge, *Nanotechnology* **2020**, 31, 292002.
- [2] J. Wang, Q. Zhou, S. Shao, A. Misra, *Mater. Res. Lett.* **2017**, 5, 1.
- [3] T. W. Barbee, *Opt. Eng.* **1986**, 25, 898.
- [4] M. N. Baibich, J. M. Broto, A. Fert, F. N. Van Dau, F. Petroff, P. Etienne, G. Creuzet, A. Friederich, J. Chazelas, *Phys. Rev. Lett.* **1988**, 61, 2472.
- [5] X. Zhang, K. Hattar, Y. Chen, L. Shao, J. Li, C. Sun, K. Yu, N. Li, M. L. Taheri, H. Wang, J. Wang, M. Nastasi, *Prog. Mater. Sci.* **2018**, 96, 217.
- [6] A. V. Druzhinin, G. Lorenzin, D. Ariosa, S. Siol, B. B. Straumal, J. Janczak-Rusch, L. P. H. Jeurgens, C. Cancellieri, *Mater. Des.* **2021**, 209, 110002.
- [7] T. Wejrzanowski, M. Lewandowska, K. Sikorski, K. J. Kurzydowski, *J. Appl. Phys.* **2014**, 116, 2.
- [8] A. V. Druzhinin, C. Cancellieri, E. A. Klyatskina, A. A. Mazilkin, N. N. Khrapova, B. B. Straumal, J. Janczak-Rusch, *Surf. Coat. Technol.* **2023**, 471, 129880.
- [9] A. V. Druzhinin, D. Ariosa, S. Siol, N. Ott, B. B. Straumal, J. Janczak-Rusch, L. P. H. Jeurgens, C. Cancellieri, *Materialia* **2019**, 7, 100400.
- [10] W. W. Mullins, *J. Appl. Phys.* **1957**, 28, 333.
- [11] A. Misra, R. G. Hoagland, *J. Mater. Res.* **2005**, 20, 2046.
- [12] F. Moszner, C. Cancellieri, M. Chiodi, S. Yoon, D. Ariosa, J. Janczak-Rusch, L. P. H. Jeurgens, *Acta Mater.* **2016**, 107, 345.
- [13] Y. J. Ma, Y. P. Cai, G. J. Wang, M. J. Cui, C. Sun, Z. H. Cao, X. K. Meng, *Mater. Sci. Eng., A* **2019**, 742, 751.
- [14] T. Niu, Y. Zhang, J. Cho, J. Li, H. Wang, X. Zhang, *Acta Mater.* **2021**, 208, 116679.
- [15] Y. Hu, G. Yang, Z. Tian, Z. Hu, *J. Alloys Compd.* **2019**, 790, 723.
- [16] C. Cancellieri, E. Klyatskina, M. Chiodi, J. Janczak-Rusch, L. Jeurgens, *Appl. Sci.* **2018**, 8, 2403.
- [17] C. Cancellieri, F. Moszner, M. Chiodi, S. Yoon, J. Janczak-Rusch, L. P. H. Jeurgens, *J. Appl. Phys.* **2016**, 120, 195107.
- [18] G. Lorenzin, M. S. Bin Hoque, D. Ariosa, L. P. H. Jeurgens, E. R. Hoglund, J. A. Tomko, P. E. Hopkins, C. Cancellieri, *Acta Mater.* **2022**, 240, 118315.
- [19] L. Romano-Brandt, E. Salvati, E. Le Bourhis, T. Moxham, I. P. Dolbnya, A. M. Korsunsky, *Surf. Coat. Technol.* **2020**, 381, 125142.
- [20] J. Yeom, G. Lorenzin, C. Cancellieri, J. Janczak-Rusch, *Mater. Lett.* **2023**, 352, 135074.
- [21] E. Chason, *Thin Solid Films* **2012**, 526, 1.
- [22] R. C. Cammarata, *Prog. Surf. Sci.* **1994**, 46, 1.
- [23] H. Li, Z. Xing, B. Li, X. Liu, B. Lehmert, M. Matthias, Z. Li, W. Tillmann, *Vacuum* **2022**, 200, 111007.
- [24] M. Chiodi, C. Cancellieri, F. Moszner, M. Andrzejczuk, J. Janczak-Rusch, L. P. H. Jeurgens, *J. Mater. Chem. C* **2016**, 4, 4927.
- [25] V. Araullo-Peters, C. Cancellieri, M. Chiodi, J. Janczak-Rusch, L. P. H. Jeurgens, *ACS Appl. Mater. Interfaces* **2019**, 11, 6605.
- [26] T. Wejrzanowski, J. Lipiecka, J. Janczak-Rusch, M. Lewandowska, *Appl. Surf. Sci.* **2019**, 493, 261.
- [27] M. Czagány, D. Varanasi, A. Sycheva, D. Janovszky, D. Koncz-Horváth, F. Kristály, P. Baumli, G. Kaptay, *J. Mater. Sci.* **2021**, 56, 7823.
- [28] F. Moszner, C. Cancellieri, C. Becker, M. Chiodi, J. Janczak-Rusch, L. P. H. Jeurgens, *J. Mater. Sci. Eng. B* **2016**, 6, 226.
- [29] B. Lehmert, J. Janczak-Rusch, G. Pigozzi, P. Zuraw, F. La Mattina, L. Wojarski, W. Tillmann, L. P. H. Jeurgens, *Mater. Trans.* **2015**, 56, 1015.
- [30] A. Kosinova, D. Wang, P. Schaaf, A. Sharma, L. Klinger, E. Rabkin, *Acta Mater.* **2018**, 149, 154.
- [31] D. Amram, O. Kovalenko, L. Klinger, E. Rabkin, *Scr. Mater.* **2015**, 109, 44.
- [32] F. Pei, E. Buchovecky, A. Bower, E. Chason, *Acta Mater.* **2017**, 129, 462.
- [33] C. D. Appleget, A. M. Hodge, *Adv. Eng. Mater.* **2019**, 21, 1801268.
- [34] A. V. Druzhinin, C. Cancellieri, R. Hauert, E. A. Klyatskina, N. N. Khrapova, A. A. Mazilkin, B. B. Straumal, J. Janczak-Rusch, *Vacuum* **2023**, 210, 111850.
- [35] D. Ariosa, C. Cancellieri, V. Araullo-Peters, M. Chiodi, E. Klyatskina, J. Janczak-Rusch, L. P. H. Jeurgens, *ACS Appl. Mater. Interfaces* **2018**, 10, 20938.
- [36] G. Abadias, E. Chason, J. Keckes, M. Sebastiani, G. B. Thompson, E. Barthel, G. L. Doll, C. E. Murray, C. H. Stoessel, L. Martinu, *J. Vac. Sci. Technol., A* **2018**, 36, 020801.
- [37] A. M. Korsunsky, *A Teaching Essay on Residual Stresses and Eigenstrains*, 1st ed., Elsevier Inc., Oxford **2017**.
- [38] M. E. Kassner, M. T. Pérez-Prado, *Fundamentals of Creep in Metals and Alloys*, Elsevier Ltd., Oxford **2004**, <https://doi.org/10.1016/B978-0-08-043637-1.X5000-5>.
- [39] E. Jiran, C. V. Thompson, *Thin Solid Films* **1992**, 208, 23.
- [40] B. Okkerse, *Phys. Rev.* **1956**, 103, 1246.
- [41] G. Rhead, *Acta Metall.* **1963**, 11, 1035.
- [42] R. E. Hoffman, D. Turnbull, *J. Appl. Phys.* **1951**, 22, 634.
- [43] J. C. M. Hwang, R. W. Balluffi, *J. Appl. Phys.* **1979**, 50, 1339.
- [44] J. C. M. Hwang, J. D. Pan, R. W. Balluffi, *J. Appl. Phys.* **1979**, 50, 1349.
- [45] M. Callisti, T. Polcar, *Acta Mater.* **2017**, 124, 247.
- [46] R. W. Balluffi, S. M. Allen, W. C. Carter, *Kinetics of Materials*, Wiley-Interscience, Massachusetts **2005**.
- [47] A. Ostrovsky, *Defect Diffus. Forum* **1998**, 156, 249.
- [48] J. Crank, *The Mathematics of Diffusion*, 2nd ed., Clarendon Press, Oxford **1975**.
- [49] *Smithells Metals Reference Book*, 8th ed. (Ed: E. A. Brandes), Elsevier, Oxford **2004**, pp. 14-1–14-45, <https://doi.org/10.1016/B978-075067509-3/50017-8>.
- [50] D. Lazarus, C. T. Tomizuka, *Phys. Rev.* **1956**, 103, 1155.

- [51] J. Sommer, C. Herzig, *J. Appl. Phys.* **1992**, 72, 2758.
- [52] P. Gumbsch, M. S. Daw, S. M. Foiles, H. F. Fischmeister, *Phys. Rev. B* **1991**, 43, 13833.
- [53] P. Wynblatt, *J. Phys. Chem. Solids* **1968**, 29, 215.
- [54] W. Triftshäuser, J. D. McGervey, *Appl. Phys.* **1975**, 6, 177.
- [55] M. I. Haftel, *Phys. Rev. B* **2001**, 64, 125415.
- [56] P. N. Ram, *Phys. Rev. B* **1988**, 37, 6783.
- [57] R. H. Rautioaho, *Phys. Status Solidi B* **1983**, 115, 95.
- [58] A. S. Berger, S. T. Ockers, R. W. Siegel, *J. Phys. F: Met. Phys.* **1979**, 9, 1023.
- [59] W. Bian, R. Li, W. Guo, H. Xue, X. Zhang, *Phys. Chem. Chem. Phys.* **2020**, 22, 27433.
- [60] D. Amram, L. Klinger, N. Gazit, H. Gluska, E. Rabkin, *Acta Mater.* **2014**, 69, 386.
- [61] J. Sommer, T. Muschik, C. Herzig, W. Gust, *Acta Mater.* **1996**, 44, 327.